Results in Engineering 15 (2022) 100598

Contents lists available at ScienceDirect

Results in Engineering

journal homepage: www.sciencedirect.com/journal/results-in-engineering

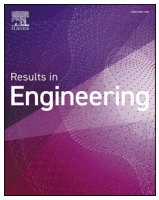

# Methane pyrolysis on sponge iron powder for sustainable hydrogen production

Mikhail S. Vlaskin [a,b,c,*], Anatoly V. Grigorenko [a], Alexander A. Gromov [d], Vinod Kumar [b,c], Alexander O. Dudoladov [a], Olga V. Slavkina [e], Viktor I. Darishchev [e]

[a] Joint Institute for High Temperatures of the Russian Academy of Sciences, 13/2 Izhorskaya St, Moscow, 125412, Russian Federation
[b] Graphic Era (Deemed to Be University), Dehradun, Uttarakhand, 248002, India
[c] Peoples' Friendship University of Russia (RUDN University), Moscow, 117198, Russian Federation
[d] National University of Science and Technology "MISIS", Moscow 119049, Russian Federation
[e] Lukoil-Engineering Llc, Pokrovsky b-r, 3 building 1, Moscow, 109028, Russian Federation

A B S T R A C T

Methane pyrolysis is one of the possible methods to produce low-carbon hydrogen. One of the most promising catalysts for methane pyrolysis is Fe due to its availability, relatively low cost and high working temperature. In the presented paper, the methane pyrolysis on unsupported (without a carrier) sponge iron in the form of powder was studied in the temperature range of 700–1100 °C. Methane pyrolysis was carried out in a stainless-steel tube reactor with an inner diameter of 10 mm. The reactor was heated locally by propane burner, the length of the heated zone was about 8 cm along the reactor tube. Methane feed rates were about 50, 100, and 200 ml/min, and the residence time of methane in the 8 cm long reaction zone was about 4, 2 and 1 s, respectively. The hydrogen yield increased with an increase in the temperature and a decrease in methane feed rate. At 700–800 °C, the hydrogen yield did not exceed 20%. At 900 °C, the yield reached 28.6% at a residence time of about 4 s. At 1000 °C, hydrogen yield was about 40 and 66.5% at a residence time of about 1 and 4 s, respectively. At 1100 °C, hydrogen yield varied in the range of 70–85%. The use of a catalyst increased the hydrogen yield by 81% compared to the experiment without a catalyst at 1100 °C. The catalytic effect of sponge iron powder can be used in the development of methane pyrolysis plants.

## 1. Introduction

Unlike hydrocarbon fuels, hydrogen combustion is not accompanied by carbon emissions into the environment [1]. Therefore, in connection with the worldwide aspiration for developing low-carbon energy, the use of hydrogen instead of traditional fuels is of great interest [2,3]. However, hydrogen is not a primary energy carrier, and to use it for energy, it must first be produced by one way or another. The main industrial method for producing hydrogen today is the steam reforming of natural gas. This process is accompanied by large emissions of carbon dioxide into the atmosphere as one of the main by-products [4]. Therefore, the production of hydrogen by this method without the use of additional measures for the utilization of carbon oxides does not satisfy the concept of low-carbon energy. Low-carbon hydrogen production can be realized by electrolysis if the electrical energy used in the electrolysis process is also obtained from a low-carbon method (based on renewable energy sources, hydroelectric power plants or nuclear power plants) [5]. However, despite the active development of electrolysis technologies, the cost of hydrogen obtained by electrolysis remains several times higher than the cost of hydrogen obtained from hydrocarbon feedstock [4].

Low-carbon hydrogen can be obtained from natural gas using preliminary thermal decomposition of natural gas and further separation of the formed carbon from hydrogen. This method is often referred to as methane pyrolysis, since the main component of natural gas is methane. The methane pyrolysis process is endothermic, for this process it must supply 75 kJ/mol of thermal energy in accordance with the following equation:

$$CH_4 \rightarrow C + 2H_2 + 75\ kJ/mol \quad (1)$$

Due to the decomposition, 1 atom of carbon and 2 molecules of hydrogen are produced from 1 molecule of methane. The calorific value of the produced 2 molecules of hydrogen is $2 \times 286 = 572$ kJ/mol:

$$2H_2 + O_2 \rightarrow 2H_2O - 572\ kJ/mol \quad (2)$$

Thus, considering the thermal energy required for the decomposition of methane, the thermal energy available for the use is (572–75) = 497 kJ/mol.

* Corresponding author. Joint Institute for High Temperatures of the Russian Academy of Sciences, 13/2 Izhorskaya St, Moscow, 125412, Russian Federation.
*E-mail address:* vlaskin@inbox.ru (M.S. Vlaskin).

https://doi.org/10.1016/j.rineng.2022.100598
Received 25 May 2022; Received in revised form 16 August 2022; Accepted 17 August 2022
Available online 22 August 2022

For comparison, the "whole" methane combustion (without preliminary decomposition) releases 891 kJ/mol:

$$CH_4 + 2O_2 \rightarrow CO_2 + 2H_2O - 891\ kJ/mol \quad (3)$$

The "loss" of the available thermal energy in the case of preliminary decomposition of methane into hydrogen and carbon and separation of the latter will be (891–497) = 394 kJ/mol, which is equal to the calorific value of the produced carbon. Carbon, which is not consumed for energy, can be used in a wide variety of industries: for the production of rubber products, varnishes, lithium-ion batteries, composite materials, graphite electrodes of electric arc furnaces, etc. [6].

Despite the relatively simple equation of the chemical reaction (1), the process of methane pyrolysis is still not enough technologically mature today. The ongoing work on methane pyrolysis can be divided into three groups: plasma-chemical decomposition, non-catalytic decomposition in molten salts or metals, and catalytic pyrolysis.

Plasma technologies for converting methane to hydrogen and carbon have several advantages. Plasma technology provides high yields of hydrogen and carbon [7]. The size of the plasma reactors is an order of magnitude smaller compared to thermal decomposition reactors. However, one of the main barriers to the industrial use of plasma pyrolysis is the high cost of relatively expensive (compared to thermal energy) electrical energy.

For the thermal non-catalytic decomposition of methane, methods based on passing it through molten metals or alloys are proposed. The process of methane decomposition by passing it through a tin melt at temperatures of 700–950 °C was studied in Ref. [8]. In another work with tin [9], the decomposition of methane was studied in the temperature range of 930–1175 °C and gas flow rates of 50–200 ml/min. The hydrogen yield increased with increasing temperature and decreasing gas flow rate; the maximum hydrogen yield of 78% was achieved at a temperature of 1175 °C at a flow rate of 50 ml/min. In Refs. [10,11], a Ni and Bi melt (27/73 mol.%) was used for the decomposition of methane. When methane was passed through gallium melt, the maximum conversion degree of 91% was achieved at a temperature of 1119 °C and a residence time in the liquid metal of about 0.5 s [12]. Several works are devoted to methane pyrolysis by bubbling in molten salts ($MnCl_2$, KCl, NaBr, KBr, NaCl) [13–15]. The main disadvantage of these methods is the difficulty of maintaining a high temperature in the volume of the melt, as well as clogging of the working volume with a carbon-based product.

To lower the operating temperature of the methane pyrolysis process and accelerate the process, various non-metallic (mainly carbon-based) and metallic catalysts are used. Various carbon materials have been studied for the pyrolysis of methane: activated carbon, technical carbon, glassy carbon, acetylene black, graphite, diamond powder, semi-coke, fullerenes, and carbon nanotubes [16]. Despite some advantages of carbon catalysts over metal ones, they are still characterized by lower catalytic activity, which entails the need to maintain higher process temperatures and holding times at high temperatures. The greatest attention among metal catalysts in research is paid to such metals as Ni, Co and Fe, due to their availability, relatively low cost, high activity and stability [17–19]. However, for industrial use, an iron catalyst is usually proposed as the cheapest and safest [16].

Usually, the iron catalyst is supported on a specific carrier. $Al_2O_3$, $SiO_2$, $ZrO_2$, $TiO_2$, $CeO_2$, $La_2O_3$, and H-ZSM-5 were used as carriers for the iron catalysts [20–27]. One of the main problems with the use of such catalysts is carbon deposition on the catalyst surface and the difficulty of its regeneration without COx emissions, as well as catalyst degradation. The separation problem could be decided more effectively if instead of supported catalysts, unsupported iron powder or granules are used in the process. The effective removal of carbon from iron could be provided by the high difference in the density of these materials (7.874 g/cm$^3$ for iron versus ~2 g/cm$^3$ for carbon). The separation process can be carried out in a separately located separation plant. The use of iron as a catalyst potentially has several advantages, such as a relatively low cost, a high working temperature, a relatively high thermal conductivity, and safety.

Studies of the methane pyrolysis on unsupported iron are limited. The pyrolysis of methane on iron without a carrier was studied in Ref. [23]. However, in this work, the study was conducted only at a temperature below 700 °C, and the hydrogen yield on unsupported iron did not exceed 20%. The pyrolysis of methane on iron without a carrier requires a more detailed study, in particular, in a wider temperature range. Moreover, the production method for the iron is often unspecified while it could influence both the kinetics of the process as well as the economic and sustainability of the methane decomposition method.

The novelty of this study is that we use sponge iron powder as a catalyst for methane pyrolysis. The use of sponge iron powder could strengthen the sustainability of the methane decomposition method because of the fact that it can be produced using fossil-free hydrogen gas, thus lowering the total $CO_2$ load. Moreover, the novelty of this study is provided by the lack of knowledge about methane pyrolysis on unsupported iron at high temperatures.

In this article, the process of methane pyrolysis on sponge iron powder in the temperature range of 700–1100 °C was studied using an original experimental plant. The pyrolysis of methane was carried out with a residence time of about 1 s in a stainless-steel tube reactor heated locally by propane burner. This work aims to determine the yield of hydrogen and the composition of the gaseous product depending on the temperature and methane feed rate. Additionally, the structure and composition of the catalyst after pyrolysis are studied and a correlation with the experimental conditions is established.

## 2. Experimental

### 2.1. Materials

The experiments were carried out on methane with a purity of 99.99 vol% (grade A) supplied by the Moscow Gas Processing Plant. Sponge iron powder with the purity of 99.38 mass. % was used as a catalyst. Sponge iron powder was supplied by Materials-K Ltd. (Russia). The chemical composition of sponge iron powder is presented in Table 1. The main impurities in iron powder are C, Si and Mn.

### 2.2. Experimental plant

Fig. 1 shows a scheme of the experimental plant used in research on methane pyrolysis on sponge iron powder. The pyrolysis reactor is a stainless steel AISI 310 tube with an inner diameter of 10 mm and a wall thickness of 1 mm. Above and below the reactor there are covers for loading the reactor with iron powder, as well as for unloading the powder and cleaning the reactor after the experiment. Methane was fed into the reactor from methane tank 1 through reducer 2 and rotameter 3 at a set flow rate. The methane feed rate is set using a fine adjustment valve built into the rotameter. Inside the reactor 4, the gas is fed into the area loaded with iron powder 7. The reactor is heated from the outside by means of a gas propane burner 14 (gas burner model is GV-3V-01). Propane is supplied to the burner from a propane tank 11 through a reducer 12. The flame of the burner flows into a T-shaped tube 5 installed on the reactor vessel in the area where iron powder is loaded. Gaseous pyrolysis products are sampled into a 1-L rubber chamber for gas chromatographic analysis. Leaving the reactor, before entering the chamber, the gas passes through a cylindrical filter 8, as a filter element

**Table 1**
Chemical composition of sponge iron powder used in experiments.

| Mass fraction, %, | | | | | |
|---|---|---|---|---|---|
| no less | no more | | | | |
| Fe | C | Si | Mn | S | P |
| 99.38 | 0.05 | 0.15 | 0.4 | 0.02 | 0.02 |

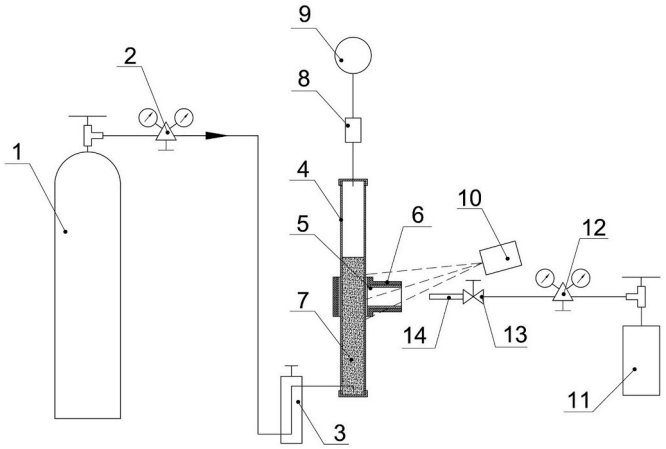


**Fig. 1.** An experimental plant for methane pyrolysis on iron powder: 1 - methane tank, 2 - reducer, 3 - rotameter, 4 - reactor, 5 - T-shaped tube, 6 - T-shaped tube thermal insulation, 7 - iron powder, 8 - filter, 9 - chamber for gas sampling, 10 - pyrometer, 11 - propane tank, 12 - reducer, 13 - propane flow control valve, 14 - propane burner.

in which there is an ash-free paper filter FM 03.14 V. The temperature of the reactor is determined using a pyrometer 10 (pyrometer model is Kelvin-compact 2300 D). The temperature is measured in three positions: directly in the heated zone, as well as above and below the T-shaped tube. The heating temperature of the reactor is controlled by increasing or decreasing the gas flow in the heating zone using the propane flow control valve 13 in the propane burner 14.

Before each experiment, a fresh iron powder in the amount of 90 g was loaded into the reactor. The height of the iron powder filling was about 30 cm. The length of the heated zone of the T-shaped tube was 8 cm.

Next, methane was fed into the reactor, followed by cold flushing of the reactor with methane at a rate of about 200 ml/min for 1 h. This purge was carried out to remove air from the reactor. Then, using a methane flow regulator (rotameter), a certain methane flow rate of about 50, 100, or 200 ml/min was set. Methane consumption was checked at the time of filling a 1-L rubber chamber installed at the outlet of the reactor. After that, the rubber chamber for gas sampling was disconnected and the heating of the reactor was started using a propane burner. The reactor was heated to temperatures of 700, 800, 900, 1000, or 1100 °C. The heating time of the reactor to a certain maximum temperature was about 4–5 min. After the maximum temperature of the reactor was established, an empty rubber chamber was connected to its outlet (through a filter) to take gas for gas chromatographic analysis. After the first chamber was filled, the second empty chamber was connected for gas intake, and after the second chamber was filled, the third empty chamber was connected for gas intake. The gas intake time for each chamber was controlled. After a successive filling of three rubber chambers, the propane supply to the propane burner was stopped. After cooling down, the reactor was opened, and the spent iron powder was sent for analysis. The chambers with gas were analyzed for gas chromatographic analysis directly after the end of sampling.

### 2.3. Methods

The chemical composition of the gas obtained due to methane pyrolysis was studied on a Khromatek-Kristall 5000 gas chromatograph. The general substances analyzed by a gas chromatograph are $H_2$, $O_2/N_2$ (air), CO, $CO_2$, $C_1$–$C_5$ hydrocarbons (paraffin-olefin class with isomers). The chromatograph includes 2 TCD (detection limit – 3 $10^{-9}$ g/ml for heptane or propane) with stainless steel columns 3 m length and inner diameter 2 mm, filled with NaX 80/100 mesh and FID (detection limit – 1.1 $10^{-12}$ g/s for carbon in hydrocarbons) with same columns, filled with HayeSep Q 80/100 mesh, a set of multiport automatic valves; the entire analysis occurs in the isothermal mode at 80 °C for about 20 min, argon as carrier gas flow rate was 15 ml/min. With a single start, programmed switching of taps occurred, and recording began for all detectors; during the analysis, the guard columns were switched and blown off. The chromatograph was calibrated with verified gas mixtures supplied from the gas chromatograph manufacturer.

The chemical composition was determined with accuracy and the limits of the permissible relative error in percentage:

- in the range from 0.0001 to 0.0010% inclusive - ± (5.1–1111 * X);
- in the range from 0.05 to 0.10% inclusive - ± (4–15.1 * X);
- in the range from 0.10 to 0.50% inclusive - ± (2.75–2.5 * X);
- in the range from 0.50 to 20.0% inclusive - ± (1.5–0.046 X);
- in the range from 20.0 to 70.0% inclusive - ± (0.76–0.008 X);
- in the range of St. 70.0–92.0% - ± (0.51–0.0045 X),

where X is the current measured value.

The microstructure of the samples of the initial iron powder and iron powder after the pyrolysis was studied on a Nova NanoSem 650 scanning electron microscope (SEM) using a ring backscattered electron detector, which makes it possible to obtain a contrast on the relief surfaces by the average atomic numbers of microstructure elements. The samples were attached to the microscope stage using an electrically conductive tape. The samples were not coated with a conductive coating to avoid possible shielding of nanoscale objects. The scanning was carried out by secondary electrons with accelerating voltages of 2 and 3 kV. To reduce the inevitable charging of the samples by the electron probe, images were acquired by multiple scans using the “drift correction” mode.

The phase composition of the iron powder after the pyrolysis was studied by X-ray diffraction on a Rigaku SmartLab SE diffractometer using CuKα radiation according to the standard method with a step of 0.02°. The phase composition of the samples was identified using Match! software.

The particle size analysis of the initial iron powder was studied by laser diffraction using a Fritsch Analysette 22 diffractometer using a semiconductor laser ($\lambda = 650$ nm, 7 mW power). Powder was fed into the measuring chamber from an ultrasonic bath automatically using a dispersing device. The calculation of the particle size distribution based on the intensity distribution was carried out according to the Mie theory. The measurement range was 0.1–600 μm. The absolute error in the integral distributions was about 5%.

The bulk density of the initial iron powder was determined using a 50 ml flask and a Sartorius Cubis MSA324S-1 CE-DA analytical balance. Iron powder was poured into a flask to the mark, followed by the measurement of the mass of the powder poured into the flask. The bulk density was determined by dividing the measured mass by the occupied volume (50 ml). The procedure for determining the bulk density of the iron powder was carried out in a 5-fold repetition.

The structural characteristics of iron powder samples were determined from nitrogen adsorption isotherms at 77 K recorded on a Nova 2200e surface area analyzer (Quantachrome, USA). Before measuring the isotherms, the samples were degassed at 250°C and a residual pressure of $10^{-3}$ mm Hg within 3 h. The surface area of the samples was calculated using the BET equation, the total pore volume was determined from the nitrogen adsorption isotherm at a relative pressure of 0.995.

High-resolution transmission electron microscopy (TEM) was used to analyze the particle surface morphology and the structure of iron powder. The samples were analyzed on an FEI Osiris transmission electron microscope with an accelerating voltage of 200 kV. The procedures for sample preparation, measurements, and image processing are similar to those described in Ref. [28].

## 3. Results and discussion

Fig. 2 shows the particle size distribution of the iron powder used as a catalyst. The maximum particle size of the iron powder was about 280 μm. The peak of the size distribution of powder particles falls on 43–45 μm, 99% of the size distribution falls on particles no larger than 164 μm.

The composition of the gas obtained from the decomposition of methane on iron powder in experiments with different temperatures and methane flow rates is shown in Table 2. The results show that with an increase in temperature and a decrease in methane flow rate, the hydrogen yield increases and the methane content decreases. In addition to methane and hydrogen, the gas produced by methane pyrolysis contains trace amounts of ethane, ethene, propane, propene, isobutane, butane and butene. At high temperatures (1000–1100 °C), the main impurity gases, except methane, are ethane and ethene.

Fig. 3 shows the yield of hydrogen in experiments on methane pyrolysis on iron powder. At temperatures of 700–800 °C, the hydrogen yield did not exceed 20%. Here, our results agree with the results obtained in Ref. [23], where the hydrogen yield on iron did not exceed 20% at temperatures of up to 700 °C. At a temperature of 900 °C, the hydrogen yield reached 28.6% at a minimum flow rate of about 50 ml/min. At a temperature of 1000 °C, the hydrogen yield was about 40% already at the maximum flow rate (about 200 ml/min) and increased to 66.5% with a decrease in the flow rate to 50 ml/min. At a temperature of 1100 °C, the hydrogen yield varied in the range of 70%–85%.

The mass fraction of the main substances in the pyrolysis product at different temperatures is shown in Fig. 4. Here, the carbon content is calculated from equation (1) and the known composition of the gaseous pyrolysis product. It can be seen that with an increase in temperature, the content of hydrogen and carbon increases, and the content of methane decreases.

Experiments on methane pyrolysis were also carried out without filling the reactor with iron powder. In experiments without iron powder, the hydrogen yield was significantly lower than in experiments with the powder. The hydrogen yield in experiments without iron powder inside the reactor did not exceed 4% at temperatures of 1000 and 1100 °C (with a methane flow rate of about 50 ml/min). This means, that the use of a catalyst increased the hydrogen yield by 81% compared to the experiment without a catalyst at 1100 °C. This result clearly proves the catalytic effect of sponge iron powder on the methane pyrolysis process.

At the same time, the catalytic activity demonstrated in this study at relatively low temperatures (700–800°C) is less than the values obtained in studies with supported Fe catalysts. For example, in Ref. [29] at 700 °C, the yield of hydrogen was about 45% using Fe/MgO catalyst. In Ref. [25], at 700 °C, the yield of hydrogen was about 80% using $Fe/Al_2O_3$ catalyst. This level of hydrogen yield in our study is achieved at higher temperatures (1000–1100 °C).

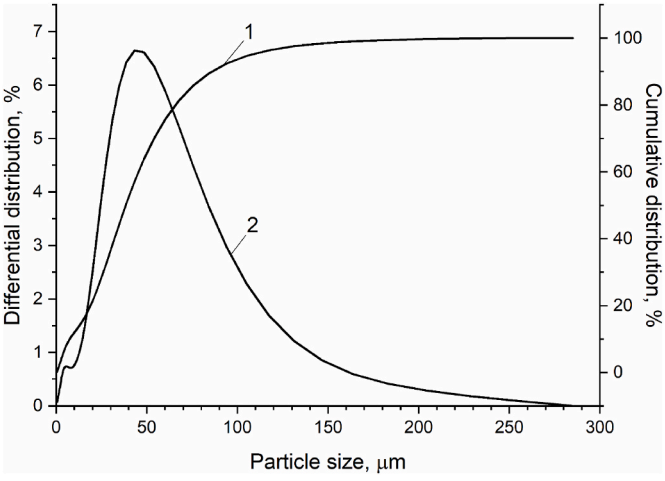


**Fig. 2.** Particle size distribution for iron powder used as a catalyst. 1 - cumulative distribution, 2 differential distribution.

After the experiments at temperatures of 1000–1100 °C, the extracted iron powder, more precisely that part of the powder that was in the heating zone (along t-shaped tube) acquired a noticeably darker shade compared to the initial one. The powder extracted from the reactor after the experiment had sintered inclusions that easily disintegrated upon pressure. BET measurements show that the iron powder has virtually no pores. The specific surface area of the powder extracted from the reactor was 0.5 $m^2/g$, and the total pore volume was 0.003 $cm^3/g$.

Fig. 5 shows SEM images of the initial iron powder and powders after experiments on methane pyrolysis at different temperatures. Phases with predominance of C in these images have a dark color, Fe - a light one. In the samples obtained at temperatures of 700–900 °C, rather rare local inclusions of layered formations based on carbon are observed on the surfaces of iron particles. Another microstructure is observed on the surfaces of iron particles obtained after experiments at temperatures of 1000 and 1100 °C, where island coatings with a carbon-based phase are seen. Generally, it can be noted that with an increase in the process temperature, the degree of coverage of iron particles by the carbon-based phase increases.

Fig. 6 shows a higher-resolution SEM image of the powder obtained in experiment at a temperature of 1100 °C and a methane flow rate of about 200 ml/min. It shows the profile of the coating of iron particles with a carbon-based phase. It can be seen that the carbon-based phase is formed predominantly in areas with surface defects. Hence, it can be assumed that the catalytic effect of iron powder on the methane pyrolysis depends on the structure of the catalyst surface.

Fig. 7 shows the XRD patterns for the samples of fresh iron powder and powders after methane pyrolysis at temperatures of 1000 and 1100 °C. The original powder does not contain other phases except for iron. Powders after pyrolysis at temperatures of 1000 and 1100 °C contain $Fe_3C$ and C, in addition to iron. From XRD analysis, it follows that the iron powder after methane pyrolysis is saturated with iron carbide $Fe_3C$, which has an orthorhombic crystal structure. The presence of carbon in the powder is insignificant due to the relatively short duration of the experiment, and it is in the amorphous state. In Ref. [30], it was shown that the peak $2\Theta = 26.5$ can correspond to graphitic carbon phase encapsulating the Fe nanoparticle core. This is confirmed by the TEM images obtained in the present work (Fig. 8). Fig. 8 shows iron particle coated with carbon.

With the increase in pyrolysis temperature, the content of iron carbide in the iron powder increases. The formation of iron carbide may change the activity of the catalyst. From the conducted experiments, we can't conclude exactly about the change in catalytic activity of the iron powder. This needs additional study. Generally, $Fe_3C$ can be formed during a wide temperature range, but $Fe_3C$ can decompose to α-Fe and carbon at 700 °C under atmospheric pressure [31] while its decomposition rate is greater than its formation rate above 725 °C [32]. The formation of $Fe_3C$ was also observed when $Fe_2O_3$–$Al_2O_3$ was reduced by $CH_4$ in Ref. [33], where $Fe_2O_3$–$Al_2O_3$ reduced by $CH_4$ showed better catalytic activity than $H_2$ due to the $Fe_3C$ generation as catalytic active sites.

Besides temperature, an important parameter of the methane pyrolysis process is the residence time of methane in the working area (heated zone). In order to estimate the residence time of methane in the working zone (t), it is necessary to know the velocity of the gas flow through the reactor tube (υ). To determine υ, it is necessary to know two parameters - the volumetric gas flow rate (Q) and the flow cross-section (S). The gas flow velocity in the tube is determined by the following equation:

$$\upsilon = \frac{Q}{S} \tag{4}$$

**Table 2**
Composition of the gas obtained by methane pyrolysis on iron powder depending on temperature and methane flow rate. At each temperature and methane flow rate, three chambers with the gaseous product were taken (one by one, without interval).

| № | Temperature, °C | Methane flow rate, ml/min | Chamber number | Composition of the obtained gas, mol. % | | | | | | | | |
|---|---|---|---|---|---|---|---|---|---|---|---|---|
| | | | | $H_2$ | $CH_4$ | $C_2H_6$ | $C_2H_4$ | $C_3H_8$ | $C_3H_6$ | $(CH_3)_3CH$ | $C_4H_{10}$ | $C_4H_8$ |
| | | | | 0.528 | 90.344 | 0.0004 | 0.0008 | 0.0002 | 0.0006 | 0.0002 | 0.0002 | 0.0008 |
| 2 | | | 2 | 0.631 | 88.018 | – | 0.0025 | 0.0003 | 0.0002 | 0.0001 | – | – |
| 3 | | | 3 | 0.794 | 89.482 | 0.0003 | 0.0002 | 0.0002 | – | – | – | – |
| 4 | | 95 | 1 | 2.560 | 87.118 | 0.0005 | 0.0013 | 0.0003 | 0.0007 | 0.0001 | 0.0001 | 0.0001 |
| 5 | | | 2 | 2.653 | 85.742 | 0.0004 | 0.0004 | 0.0002 | 0.0002 | 0.0001 | 0.0001 | – |
| 6 | | | 3 | 3.080 | 87.201 | 0.0003 | 0.0003 | 0.0002 | 0.0001 | 0.0001 | 0.0001 | – |
| 7 | | 54 | 1 | 3.304 | 85.51 | 0.0007 | 0.0024 | 0.0004 | 0.0013 | – | – | – |
| 8 | | | 2 | 3.366 | 83.792 | 0.0004 | 0.0005 | 0.0001 | 0.0002 | – | – | – |
| 9 | | | 3 | 5.149 | 82.757 | 0.0004 | 0.0005 | 0.0002 | 0.0001 | – | 0.0001 | – |
| 10 | 800 | 200 | 1 | 4.975 | 77.789 | 0.0009 | 0.0012 | 0.0002 | 0.0004 | – | 0.0001 | – |
| 11 | | | 2 | 6.383 | 83.362 | 0.0010 | 0.0007 | 0.0002 | 0.0001 | – | – | – |
| 12 | | | 3 | 5.709 | 85.221 | 0.0007 | 0.0005 | – | – | – | – | – |
| 13 | | 87 | 1 | 10.330 | 77.173 | 0.0020 | 0.0043 | 0.0003 | 0.0016 | – | 0.0001 | 0.0003 |
| 14 | | | 2 | 12.649 | 74.791 | 0.0017 | 0.0016 | 0.0001 | 0.0002 | – | – | – |
| 15 | | | 3 | 13.068 | 75.969 | 0.0014 | 0.0012 | – | 0.0002 | – | – | – |
| 16 | | 51 | 1 | 14.348 | 71.614 | 0.0021 | 0.0032 | 0.0002 | 0.0009 | – | – | 0.0001 |
| 17 | | | 2 | 14.653 | 71.824 | 0.0012 | 0.0011 | – | 0.0002 | – | – | – |
| 18 | | | 3 | 16.303 | 70.334 | 0.0012 | 0.0010 | 0.0001 | 0.0002 | – | – | – |
| 19 | 900 | 200 | 1 | 7.400 | 82.889 | 0.0013 | 0.0012 | 0.0001 | 0.0004 | 0.0001 | 0.0001 | – |
| 20 | | | 2 | 7.508 | 80.294 | 0.0011 | 0.0008 | 0.0001 | 0.0001 | 0.0001 | – | – |
| 21 | | | 3 | 8.226 | 82.910 | 0.0010 | 0.0007 | 0.0002 | 0.0001 | 0.0001 | – | – |
| 22 | | 100 | 1 | 17.376 | 68.910 | 0.0019 | 0.0012 | 0.0001 | 0.0001 | – | – | – |
| 23 | | | 2 | 20.800 | 69.169 | 0.0016 | 0.0011 | 0.0001 | 0.0001 | – | – | – |
| 24 | | | 3 | 23.187 | 65.426 | 0.0015 | 0.0009 | – | 0.0002 | – | – | – |
| 25 | | 50 | 1 | 27.021 | 62.061 | 0.0101 | 0.0470 | 0.0156 | 0.0013 | 0.0001 | – | – |
| 26 | | | 2 | 28.595 | 61.040 | 0.0023 | 0.0021 | 0.0120 | – | – | – | – |
| 27 | | | 3 | 28.000 | 57.590 | 0.0013 | 0.0009 | – | – | – | – | – |
| 28 | 1000 | 200 | 1 | 33.191 | 61.719 | 0.0026 | 0.0026 | – | 0.0006 | – | – | 0.0001 |
| 29 | | | 2 | 39.808 | 52.858 | 0.0015 | 0.0008 | – | 0.0001 | – | – | – |
| 30 | | | 3 | 39.967 | 52.001 | 0.0014 | 0.0008 | – | 0.0001 | – | – | – |
| 31 | | 111 | 1 | 50.017 | 39.142 | 0.0033 | 0.0028 | 0.0001 | 0.0004 | – | – | 0.0001 |
| 32 | | | 2 | 56.502 | 33.252 | 0.0012 | 0.0006 | – | – | – | – | – |
| 33 | | | 3 | 57.565 | 33.489 | 0.0010 | 0.0005 | – | – | – | – | – |
| 34 | | 48 | 1 | 65.651 | 14.792 | 0.0007 | 0.0008 | – | 0.0003 | – | – | – |
| 35 | | | 2 | 66.521 | 19.539 | 0.0004 | 0.0003 | – | – | – | – | – |
| 36 | | | 3 | 60.965 | 14.137 | 0.0003 | 0.0003 | – | – | – | – | – |
| 37 | 1100 | 200 | 1 | 71.825 | 16.286 | 0.0010 | 0.0007 | – | – | – | – | – |
| 38 | | | 2 | 79.743 | 8.911 | 0.0005 | 0.0002 | – | – | – | – | – |
| 39 | | | 3 | 79.295 | 5.902 | – | – | – | – | – | – | – |
| 40 | | 100 | 1 | 70.588 | 8.709 | 0.0008 | 0.0009 | 0.0003 | – | – | – | 0.0003 |
| 41 | | | 2 | 84.640 | 1.015 | – | – | – | – | – | – | – |
| 42 | | | 3 | 82.235 | 2.519 | – | – | – | – | – | – | – |
| 43 | | 53 | 1 | 83.818 | 0.260 | – | – | – | – | – | – | – |
| 44 | | | 2 | 78.437 | 1.410 | 0.0002 | 0.0003 | – | – | – | – | – |
| 45 | | | 3 | 82.463 | 0.228 | – | – | – | – | – | – | – |

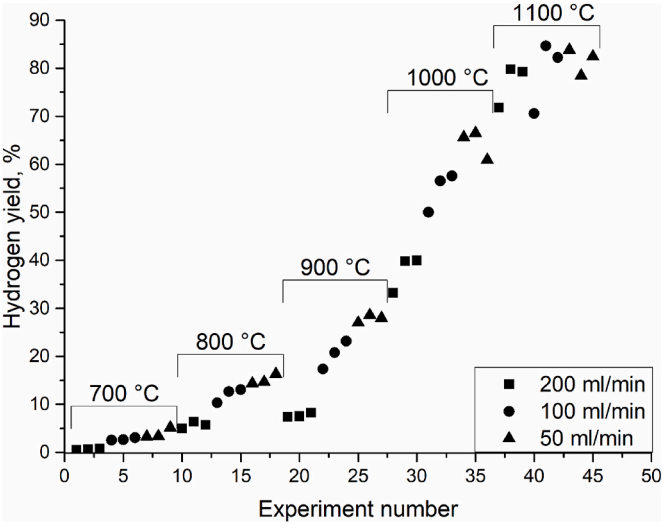


**Fig. 3.** Hydrogen yield in experiments on methane pyrolysis on iron powder.

The gas flow rate (Q) in each experiment was known, but it was determined at room temperature. In the heated zone, the volumetric gas flow rate increases, because when heated, the gas expands according to the law $\frac{V}{T} = const$. Due to the lack of accurate data on the distribution of the gas temperature inside the reactor along its length, we will further evaluate the gas flow velocity below, i.e. not taking into account the heating of the gas.

The gas flow velocity is easily calculated for a tube without powder:

$$v = \frac{Q}{S_0} = \frac{4Q}{\pi d^2}$$

where, $S_0$ is the flow area ofthe reactor tube (without powder), $d$ is the inner diameter of the reactor tube. However, in a tube with a powder, the flow area is obviously less than in an empty tube, which means that the gas flow velocity is higher in this case.

To determine the gas flow velocity through a tube filled with powder, the value of the bulk density of iron powder ($\rho$) is required. The bulk density of iron powder according to the results of our own measurements was $3.867 \pm 0.093$ g/cm$^3$.

The weight of the iron powder can be written as follows:

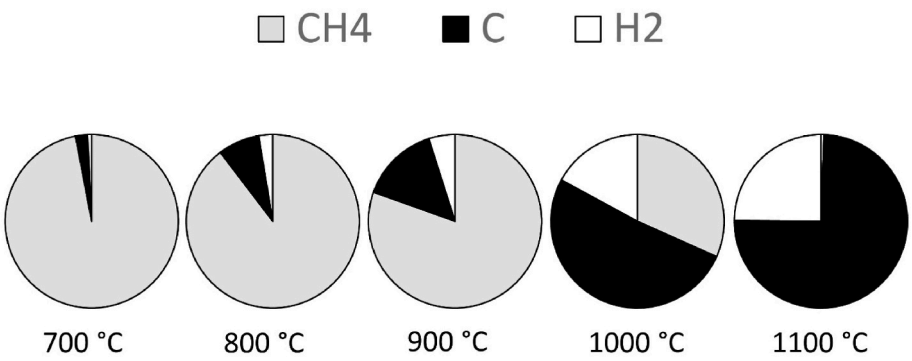


**Fig. 4.** Mass fraction of the substance in the product of pyrolysis at different temperatures: 700, 800, 900, 1000 and 1100 °C (in experiment number 9, 18, 27, 36, 45, respectively).

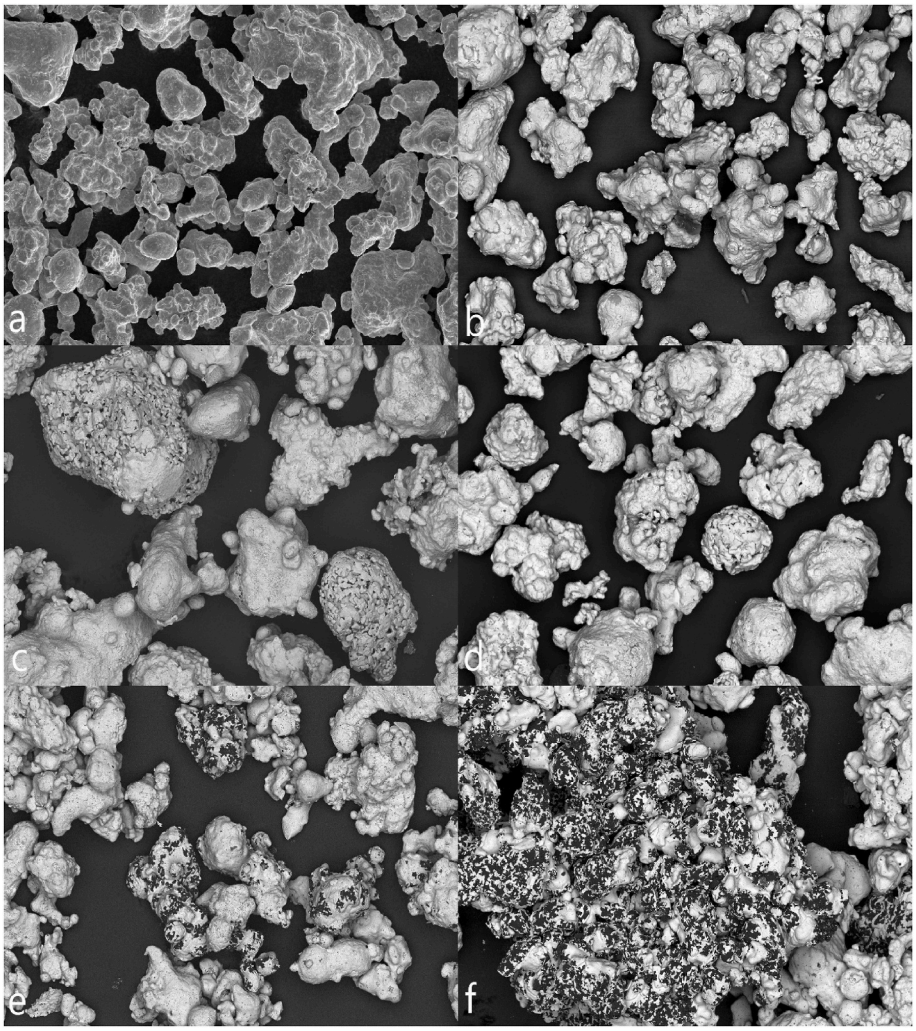


**Fig. 5.** SEM images of the initial iron powder and powders after experiments on methane pyrolysis at different temperatures: a) the initial powder, b) powder obtained in the experiment at a temperature of 700 °C, c) powder obtained in the experiment at a temperature of 800 °C, d) powder obtained in an experiment at a temperature of 900 °C, e) powder obtained in an experiment at a temperature of 1000 °C, f) powder obtained in an experiment at a temperature of 1100 °C.

$$\rho(V_{Fe} + V^{'})g = \rho_{Fe} V_{Fe} g \tag{5}$$

where $V_{Fe}$ is the volume occupied by iron particles in the powder, $V^{'}$ is the volume occupied by emptiness in the powder, $\rho_{Fe}$ is the pycnometric density of iron (7.874 g/cm3), $g$ is the acceleration of gravity.

In equation (5), the volume can be expressed in terms of area and height as follows:

$$\rho h(S_{Fe} + S^{'}) = \rho_{Fe} h S_{Fe}$$

whence the following equation follows:

$$\frac{S^{'}}{S_{Fe}} = \frac{\rho_{Fe}}{\rho} - 1 \tag{6}$$

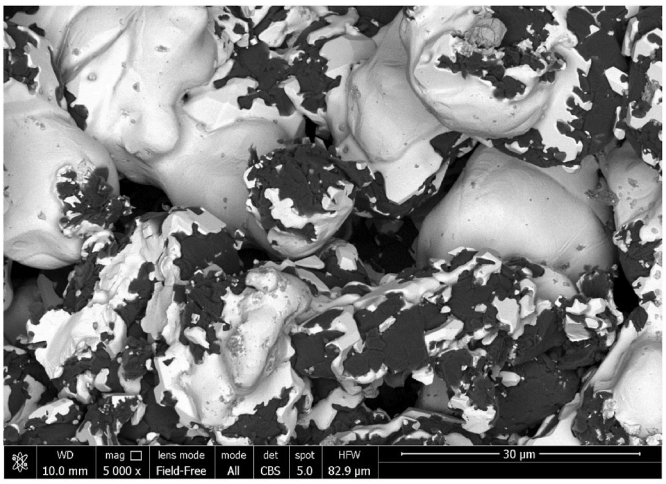


**Fig. 6.** SEM image of a sample obtained at a temperature of 1100 °C and methane flow rate of about 200 ml/min at higher resolution.

where $S_{Fe}$ is the area of the tube cross-section occupied by iron particles, $S'$ is the area of the tube cross-section occupied by the emptiness through which the gas flows. For $S_{Fe}$ and $S'$ this equation is valid:

$$S_{Fe} + S' = S_0 \tag{7}$$

Solving the system of equations (6) and (7), one can determine the required $S'$:

$$S' = S_0 \frac{\rho_{Fe} - \rho}{\rho_{Fe}} \tag{8}$$

By substituting the values of the bulk density of the iron powder and pycnometric density of iron, one can find the area in the tube section occupied by the emptiness, i.e. the area over which the gas flows. By substituting the value of $S'$ in equation (4), one can determine the gas flow velocity for the tube with the powder:

$$v = \frac{Q}{S'}$$

By substituting in (8) the values $\rho = 3.867$ g/cm$^3$ and $\rho_{Fe} = 7.874$ g/cm$^3$, one obtains that $S' \approx 0.5S_0$.

Table 3 shows the values of the flow velocity of methane in the tube without powder and with powder depending on the volumetric flow rate of methane. From the calculations, it follows that the methane flow velocity in the tube with iron powder increased from 2.12 to 8.48 cm/s with an increase in the volumetric flow rate from 50 to 200 ml/min.

The residence time in the heated zone is determined by the length of this zone. Table 3 shows the estimated holding time of methane in an 8 cm zone of the reactor (8 cm is the length of the T-shaped tube along the reactor tube). From the calculated data, it follows that the residence time in the 8-cm heated zone in the tube with iron powder decreased from 3.78 to 0.94 s with an increase in the methane flow rate from 50 to 200 ml/min. The values presented in Table 3 are only the estimate from above of the residence time of methane in an 8 cm-heated zone of the reactor tube. Along the length of the reactor tube, a high-gradient temperature field was established in the experiment. Generally, the results obtained are in agreement with the results of other studies. In particular, with the results of [12], where at a temperature of 1119 °C and a residence time of about 0.5 s (in a gallium melt) the maximum degree of methane conversion was 91%.

Generally, our results are in a good agreement with those results of [34], where the kinetics of the methane pyrolysis process was studied. In accordance with [34], the mole fraction of hydrogen produced from the decomposition of methane at 1100 °C and 1 bar is about 0.7. This is lower than the values obtained in our work. This could be explained by

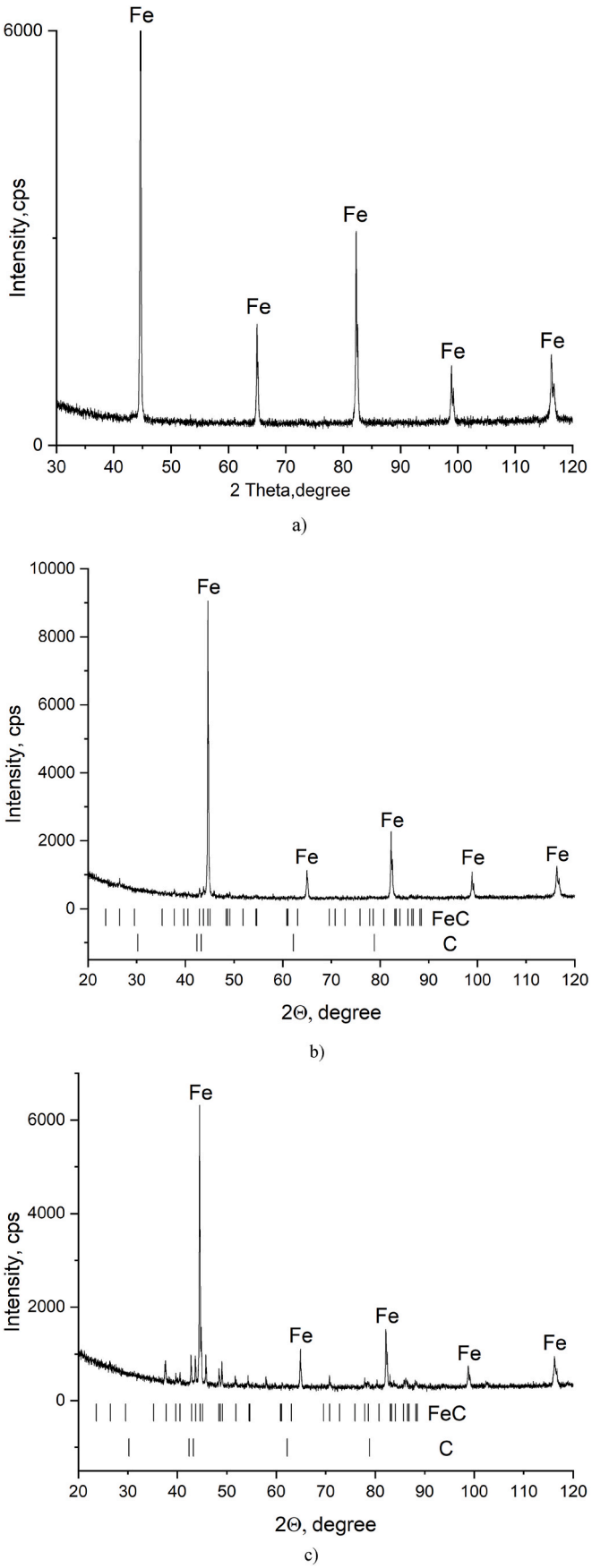


**Fig. 7.** XRD patterns for the samples of iron powder after methane pyrolysis at temperatures of 1000 (a) and 1100 (b) °C.

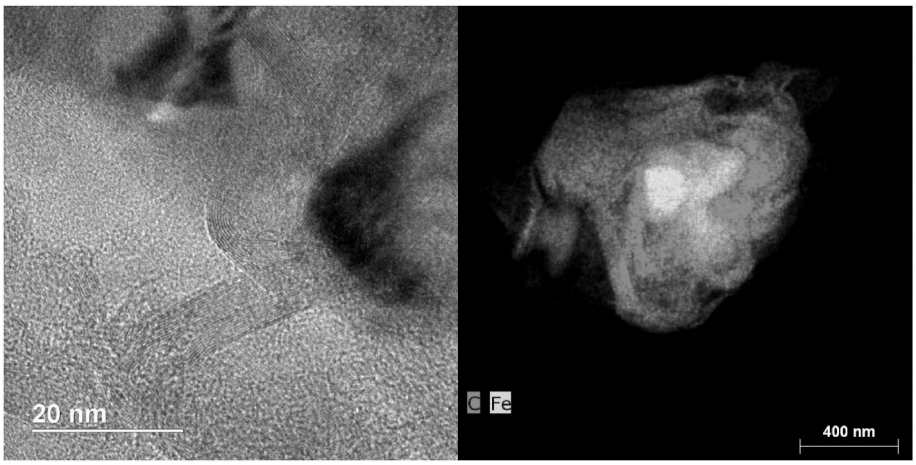


**Fig. 8.** The TEM image of a sample obtained at a temperature of 1100 °C.

**Table 3**
Values of the methane flow velocities in the tube without powder and with powder (without taking into account the thermal expansion of the gas), as well as the calculated residence time of methane in the 8 cm heated zone of the reactor (8 cm is the length of the T-shaped tube along the reactor tube).

| Methane feed rate, ml/min | Methane flow velocity in the tube without powder, cm/sec | Methane flow velocity in a tube with Fe powder, cm/sec | Residence time in an 8-cm heated zone in a tube without powder, sec | Residence time in an 8-cm heated zone in a tube with Fe powder, sec |
|---|---|---|---|---|
| 50 | 1,06 | 2,12 | 7,54 | 3,78 |
| 100 | 2,12 | 4,24 | 3,78 | 1,89 |
| 200 | 4,24 | 8,48 | 1,89 | 0,94 |

the catalyst use in this study.

In the experiments carried out in this work, at the top and bottom of the T-shaped tube, the temperature of the reactor tube was significantly lower than that achieved directly in the heating zone. Fig. 9 shows the temperature values at the top and bottom of the T-shaped tube, as well as directly in the heating zone. Note that the temperature measured by the pyrometer on the outer surface of the tube in the heating zone is maximum, i.e. above and below the heating zone, as well as inside the tube with the powder, the temperature is below this maximum temperature. Inside the tube with the powder, an asymmetric temperature field is formed with maximum temperatures near the region of the tube wall to which the combustion products are supplied from the propane burner.

It should be noted once again that the obtained values of the velocity for the experimental conditions are only an estimate below, since the velocity of gas flow in the heated zone has been exceeding the obtained value due to the thermal expansion of the gas. Consequently, the obtained values of the residence time of the gas in the heated zone are also an estimate from above. The real residence time in the reaction zone should be less than the values indicated in Table 3.

Fig. 10 shows a schematic block diagram of an industrial methane pyrolysis plant. The key element of this plant is the reactor, in which the process of decomposition of the gaseous hydrocarbon into carbon and hydrogen occurs. However, an important element of this plant is the unit for separating the catalyst from the carbon. By using the catalyst in the form of iron powder or granules, the process of separating carbon from the catalyst should be facilitated by the difference in density between these substances. Due to the fact that the weight of iron particles significantly exceeds the weight of carbon particles formed during pyrolysis, it is possible to effectively organize the separation of these particles. This separation process can be carried out in a gas stream, while the produced hydrogen can be used as the working gas. The results of this study showed that in the process of methane pyrolysis, the surface of the iron particles is covered with iron carbide. Therefore, over time, the catalyst may fail or be consumed, for which it should be possible to

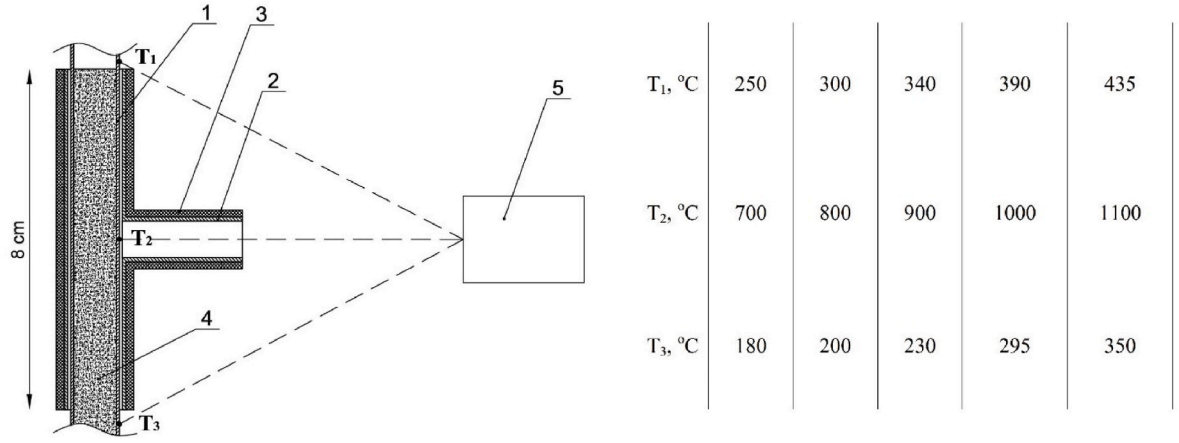


**Fig. 9.** T-shaped tube and the temperature values above and below the T-shaped tube, as well as directly in the heating zone. 1 - reactor wall, 2 - T-shaped tube, 3 - thermal insulation, 4 - iron powder, 5 - pyrometer. $T_1$ is the temperature of the reactor wall at the top of the T-shaped tube, $T_2$ is the temperature of the reactor wall in the heating zone, $T_3$ is the temperature of the reactor wall at the bottom of the T-shaped tube.

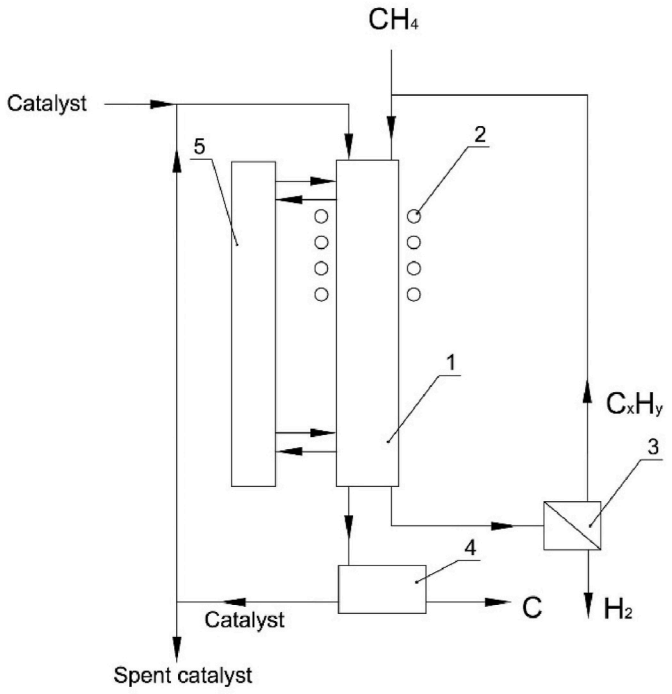


**Fig. 10.** Block diagram of an industrial methane pyrolysis plant. 1 - reactor, 2 - heat source, 3 - unit for separating undecomposed gaseous hydrocarbons from hydrogen, 4 - unit for separating catalyst from carbon, 5 - heat exchanger for heat recovery from a heated catalyst to a heated one.

introduce new portions of the catalyst and remove the spent catalyst. The block diagram in Fig. 10 contains a unit for separating hydrogen from undecomposed gaseous hydrocarbons. Such a unit may represent a Pressure Swing Adsorption unit to produce high purity hydrogen [12, 35]. After separation, hydrogen should be sent to the consumer or for further processing (use), while undecomposed gaseous hydrocarbons should be returned to the cycle.

## 4. Conclusions

The article demonstrates the possibility of obtaining hydrogen with a yield of about 80% in the process of methane pyrolysis on powdered sponge iron heated to a temperature of 1100 °C for a time of about 1 s. It was shown that with an increase in the pyrolysis temperature from 700 to 1100 °C, the hydrogen yield increased from 3% to 5% up to 85%. The hydrogen yield increases, and the methane content in gaseous products decreases, with an increase in temperature and a decrease in methane feed rate.

It was shown that after the experiments on methane pyrolysis, obtained iron powders were coated with a carbon-based phase. The carbon-based phase was formed on the surface of iron particles mainly in places with surface defects. Results of XRD analysis showed that iron powder after methane pyrolysis was saturated with iron carbide with the formula of $Fe_3C$. The most important thing to determine then is whether the catalyst material can sustain the reactivity for a long period. It is necessary to continue research and get the $H_2$ yield data for a longer period to understand how long it will retain the reactivity.

Further work on the production of hydrogen by the pyrolysis of methane should be devoted to solving the issue of separation of the formed carbon from the catalyst or to developing technical solutions for removing carbon from the working zone of the reactor. These problems seem to be the most urgent, even more urgent than the selection of the chemical composition of one or another catalyst itself. The solution to these problems requires technological elaboration. The main problem in resolving these issues is associated with high temperatures of the pyrolysis process, which entails difficulties in the selection of suitable materials and technical solutions.

## Credit author statement

**Mikhail S. Vlaskin**: Conceptualization, Methodology, Writing - Review & Editing; **Anatoly V. Grigorenko**: Visualization, Investigation; **Alexander A. Gromov**: Data Curation; **Vinod Kumar**: Writing - Review & Editing; **Alexander O. Dudoladov**: Visualization, Writing - Original Draft; **Olga V. Slavkina**: Investigation; **Viktor I. Darishchev**: Investigation, Writing - Review & Editing;

## Declaration of competing interest

The authors declare that they have no known competing financial interests or personal relationships that could have appeared to influence the work reported in this paper.

## Acknowledgment

The study was supported by a grant of Russian Science Foundation No. 21-19-00390, https://rscf.ru/project/21-19-00390/

## References

[1] N. Ripoll, M. Toledo, Results in Engineering 12 (2021), 100287.
[2] E.I. Shkolnikov, A.Z. Zhuk, M.S. Vlaskin, Renew. Sustain. Energy Rev. 15 (2011) 4611–4623.
[3] J.J. Hernández, C. Fúnez, Results in Engineering 13 (2022), 100327.
[4] P. Breeze, in: P. Breeze (Ed.), In Chapter 8 - Hydrogen Energy Storage, Academic Press, 2018, pp. 69–77.
[5] E. Amores, M. Sánchez-Molina, M. Sánchez, Results in Engineering 10 (2021), 100235.
[6] R&D Opportunities for Development of Natural Gas Conversion Technologies for Co-production of Hydrogen and Value-Added Solid Carbon Products, Argonne National Laboratory and Pacific Northwest National Laboratory Operated for the U.S. Department of Energy Office of Science (2017)..
[7] A. Mašláni, M. Hrabovský, P. Křenek, M. Hlína, S. Raman, V.S. Sikarwar, M. Jeremiáš, Int. J. Hydrogen Energy 46 (2021) 1605–1614.
[8] M. Plevan, T. Geißler, A. Abánades, K. Mehravaran, R.K. Rathnam, C. Rubbia, D. Salmieri, L. Stoppel, S. Stückrad, T. Wetzel, Int. J. Hydrogen Energy 40 (2015) 8020–8033.
[9] T. Geißler, A. Abánades, A. Heinzel, K. Mehravaran, G. Müller, R.K. Rathnam, C. Rubbia, D. Salmieri, L. Stoppel, S. Stückrad, A. Weisenburger, H. Wenninger, T. Wetzel, Chem. Eng. J. 299 (2016) 192–200.
[10] D.C. Upham, V. Agarwal, A. Khechfe, Z.R. Snodgrass, M.J. Gordon, H. Metiu, E. W. McFarland, Science 358 (2017) 917–921.
[11] N. Rahimi, D. Kang, J. Gelinas, A. Menon, M.J. Gordon, H. Metiu, E.W. McFarland, Carbon 151 (2019) 181–191.
[12] B.J. Leal Pérez, J.A. Medrano Jiménez, R. Bhardwaj, E. Goetheer, M. van Sint Annaland, F. Gallucci, Int. J. Hydrogen Energy 46 (2021) 4917–4935.
[13] D. Kang, N. Rahimi, M.J. Gordon, H. Metiu, E.W. McFarland, Appl. Catal. B Environ. 254 (2019) 659–666.
[14] C.F. Patzschke, B. Parkinson, J.J. Willis, P. Nandi, A.M. Love, S. Raman, K. Hellgardt, Chem. Eng. J. 414 (2021), 128730.
[15] B. Parkinson, C.F. Patzschke, D. Nikolis, S. Raman, D.C. Dankworth, K. Hellgardt, Int. J. Hydrogen Energy 46 (2021) 6225–6238.
[16] N. Sánchez-Bastardo, R. Schlögl, H. Ruland, Chem. Ing. Tech. 92 (2020) 1596–1609.
[17] A. Venugopal, S. Naveen Kumar, J. Ashok, D. Hari Prasad, V. Durga Kumari, K.B. S. Prasad, M. Subrahmanyam, Int. J. Hydrogen Energy 32 (2007) 1782–1788.
[18] A.F. Cunha, J.J.M. Órfão, J.L. Figueiredo, Int. J. Hydrogen Energy 34 (2009) 4763–4772.
[19] A.F. Cunha, J.J.M. Órfão, J.L. Figueiredo, Fuel Process. Technol. 90 (2009) 1234–1240.
[20] L. Zhou, L.R. Enakonda, M. Harb, Y. Saih, A. Aguilar-Tapia, S. Ould-Chikh, J.-l. Hazemann, J. Li, N. Wei, D. Gary, P. Del-Gallo, J.-M. Basset, Appl. Catal. B Environ. 208 (2017) 44–59.
[21] L. Zhou, L.R. Enakonda, Y. Saih, S. Loptain, D. Gary, P. Del-Gallo, J.-M. Basset, ChemSusChem 9 (2016) 1243–1248.
[22] I.W. Wang, D.A. Kutteri, B. Gao, H. Tian, J. Hu, Energy Fuel. 33 (2019) 197–205.
[23] A.A. Ibrahim, A.S. Al-Fatesh, W.U. Khan, M.A. Soliman, R.L. AL Otaibi, A. H. Fakeeha, J. Chin. Chem. Soc. 62 (2015) 592–599.
[24] M. Pudukudy, Z. Yaakob, Q. Jia, M.S. Takriff, Appl. Surf. Sci. 467–468 (2019) 236–248.
[25] A.S. Al-Fatesh, A.H. Fakeeha, A.A. Ibrahim, W.U. Khan, H. Atia, R. Eckelt, K. Seshan, B. Chowdhury, J. Saudi Chem. Soc. 22 (2018) 239–247.

[26] A.H. Fakeeha, S.O. Kasim, A.A. Ibrahim, A.S. Al-Awadi, E. Alzahrani, A. E. Abasaeed, A.E. Awadallah, A.S. Al-Fatesh, Front. Chem. 8 (2020).
[27] F. Al-Mubaddel, S. Kasim, A.A. Ibrahim, A.S. Al-Awadi, A.H. Fakeeha, A.S. Al-Fatesh, Catalysts 10 (2020) 793.
[28] A.V. Drakon, A.V. Eremin, E.V. Gurentsov, E.Y. Mikheyeva, R.N. Kolotushkin, Appl. Phys. B 127 (2021) 81.
[29] A.H. Fakeeha, A.A. Ibrahim, M.A. Naeem, W.U. Khan, A.E. Abasaeed, R.L. Alotaibi, A.S. Al-Fatesh, Catalysis for Sustainable Energy 2 (2015) 71–82.
[30] R. Kundu, V. Ramasubramanian, S.T. Neeli, H. Ramsurn, Energy Fuel. 35 (2021) 13523–13533.
[31] A. Tsuzuki, S. Sago, S.I. Hirano, S. Naka, JMatS 19 (1984) 2513–2518.
[32] W. Arabczyk, W. Konicki, U. Narkiewicz, I. Jasińska, K. Kałucki, Appl. Catal. Gen. 266 (2004) 135–145.
[33] P. Yan, K. Zhang, Y. Peng, Chem. Eng. Sci. 250 (2022), 117410.
[34] M. Younessi-Sinaki, E.A. Matida, F. Hamdullahpur, Int. J. Hydrogen Energy 34 (2009) 3710–3716.
[35] S. Schneider, S. Bajohr, F. Graf, T. Kolb, ChemBioEng Reviews 7 (2020) 150–158.